Reduced axonal diameter of peripheral nerve fibers in a mouse model of Rett syndrome

Noha G. Bahey[1,2,] Kamal K.E. Gadalla[1,3], Rhona McGonigal [4], Mark E. S. Bailey [5], Julia M. Edgar [4], and Stuart R. Cobb[1]

[1]Institute of Neuroscience and Psychology, University of Glasgow, [2]Histology Department, Faculty of Medicine, Tanta University, Egypt, [3]Pharmacology Department, Faculty of Medicine, Tanta University, Egypt, [4]Institute of Infection, Immunity and Inflammation College of Medical, Veterinary and Life Sciences University of Glasgow, [5]School of Life Sciences, College of Medical, Veterinary and Life Sciences, University of Glasgow.

Abstract

Rett syndrome (RTT) is a neurological disorder characterized by motor and cognitive impairment, autonomic dysfunction and a loss of purposeful hand skills. In the majority of cases, typical RTT is caused by *de novo* mutations in the X-linked gene, *MECP2*. Alterations in the structure and function of neurons within the central nervous system of RTT patients and *Mecp2*-null mouse models are well established. In contrast, few studies have investigated the effects of MeCP2-deficiency on peripheral nerves. In this study, we conducted detailed morphometric as well as functional analysis of the sciatic nerves of symptomatic adult female *Mecp2*$^{+/-}$ mice. We observed a significant reduction in the mean diameter of myelinated nerve fibers in *Mecp2*$^{+/-}$ mice. In myelinated fibers, mitochondrial densities per unit area of axoplasm were significantly altered in *Mecp2*$^{+/-}$ mice. However, conduction properties of the sciatic nerve of *Mecp2* knockout mice were not different from control. These subtle changes in myelinated peripheral nerve fibers in heterozygous *Mecp2* knockout mice could potentially explain some RTT phenotypes.

Keywords; Rett syndrome, *MECP2*, sciatic nerve, mitochondria.

Introduction

Rett syndrome (RTT; MIM 312750) is a neurological disorder characterized by a suite of motor and intellectual impairments with overt onset several months postnatally (Neul et al., 2010). In the vast majority of cases, typical RTT is caused by *de novo* loss-of-function mutations in the *MECP2* gene (reviewed in (Gadalla et al., 2011; Lyst and Bird, 2015; Leonard et al., 2017). Several mouse models of RTT have been generated (Chen et al., 2001; Guy et al., 2001; Shahbazian et al., 2002) and have been shown to recapitulate many of the features of RTT. Human postmortem studies report a range of structural changes in the RTT brain including reduced brain size and weight, reduced dendritic branching complexity and changes in spine density and morphology (Armstrong et al., 1995; Bauman et al., 1995). Similar observations have been reported in *Mecp2*-null mice (Chen et al., 2001; Nguyen et al., 2012; Robinson et al., 2012). Several studies have reported axonal neuropathy, degenerative changes and reduced numbers of large myelinated fibers in peripheral nerves in RTT patients (Haas and Love, 1988; Wakai et al., 1990), as well as mitochondrial structural abnormalities in both nerve (Wakai et al., 1990) and skeletal muscle (Ruch et al., 1989). However, no studies have yet investigated the structure and function of peripheral nerves in mouse models of RTT. These nerves can be rapidly fixed, thus preserving ultrastructural features, and changes can be quantified making them useful in the study of the human disease. In this report, we have assessed structural and functional properties of the sciatic nerve from symptomatic heterozygous *Mecp2*$^{+/-}$ mice, an accurate genetic model of RTT, using light and electron microscopy and *ex vivo* electrophysiology. The results demonstrate subtle structural changes in myelinated fibers that could potentially contribute to peripheral neuropathies in Rett syndrome, as previously inferred from human studies (Wakai et al., 1990).

Material and methods

Animals

All experiments were carried out in accordance with the European Communities Council Directive (86/609/EEC) and within the terms of a project license under the UK Animals (Scientific Procedures) Act (1986). *Mecp2*-null (*Mecp2*$^{tm1.1Bird}$) mice, originally provided as a kind gift from Professor Adrian Bird (University of Edinburgh), were maintained on a C57BL/6 background. Experimental cohorts of *Mecp2*$^{+/-}$ mice were generated by crossing *Mecp2*$^{+/-}$ females with wild-type *Mecp2*$^{+/y}$ males. Animals were maintained on 12-hour light/dark cycles with free access to normal mouse food. Mice were genotyped and scored for Rett-like phenotypes using an observational scale for mobility, gait, hindlimb clasping, abnormal breathing, tremor and general condition, as described previously (Guy et al., 2007). Unlike the male knockout (*Mecp2*$^{-/y}$) mice, which develop RTT-like phenotypes very early in life, female heterozygotes (*Mecp2*$^{+/-}$) variably develop these phenotypes later in their life (Guy et al., 2007). Therefore, this scoring system was used primarily to ensure that *Mecp2*$^{+/-}$ mouse cohort in this study had reached the symptomatic phase of the disorder.

Light and electron microscopy analysis

Mecp2$^{+/-}$ and wild-type (WT) female mice (8-9 months) were humanely sacrificed by cervical dislocation and the left sciatic nerve was exposed through a lateral incision in the mid-thigh. The proximal one-third of the nerve segment was dissected and immediately fixed in 2% paraformaldehyde + 2.5% glutaraldehyde in 0.1M phosphate buffer (pH 7.4) for 1hr at room temperature. The nerve segments were then cut transversely into small (~1mm) blocks and placed in the same fresh fixative for an additional 12 hrs at 4°C. The nerve samples were then washed with

0.1 phosphate buffer (3x15mins) and post-fixed in 1% osmium tetroxide in phosphate buffered solution for 25 mins at room temperature. Subsequently, the samples were washed in de-ionized H_2O (3x10 mins) and gradually dehydrated in the following concentrations of acetone; 70% for 20 mins, 90% for 20 mins and 100% acetone for 45 mins (3 washes of 15 mins each). Following dehydration, samples were incubated overnight in 1:1 (v/v) Durcupan (Sigma, UK)/ acetone (100%) mixture and then in 3:1 (v/v) Durcupan / acetone (100%) mixture for 3 hrs. The vials containing the samples were kept open to the air for at least 30 mins to evaporate the acetone, and this was followed by an incubation in fresh pure Durcupan for 24 hrs. This last step was repeated twice. Finally, the samples were embedded in a flat mould filled with fresh pure Durcupan and cured at 68°C for 48 hrs.

Transverse semi-thin (0.5 μm) sections of sciatic nerve were cut using a glass knife. The sections were deposited in a drop of distilled H_2O onto agar coated glass slides and dried on a hot plate at 90°C. The slides were subsequently cooled to room temperature before staining sections with Azure blue (1%) on a hot plate at 90°C (until a green ring appeared around the staining drop). The slides were rinsed with distilled H_2O to remove the excess stain and left to dry at room temperature. The sections were then dehydrated in an ascending range of ethanol solutions; 70%, 90% and finally 100% (3 times, 5 mins each), then cleared in Histo-clear (2 x 5 mins; Agar Scientific, UK) before being mounted using Histo-mount (Agar Scientific, UK) and visualized by light microscopy. Images were captured using an AxioCam MRc digital camera (Zeiss, Cambridge, UK) mounted on a light microscope (Zeiss Axioscop50, Cambridge, UK).

For analysis of nerve fiber morphology, random non-overlapping areas of interest (AOI; n =10) were acquired for each mouse sample using a 100X oil objective.

Digital images were used to assess fiber size, density and g-ratio (the ratio of the axon diameter to the fiber [axon plus myelin sheath] diameter), which provides a measure of myelin thickness relative to axonal diameter (Gillespie and Stein, 1983; Michailov et al., 2004). Measurements of fiber and axon diameter were conducted, blinded to genotype, by tracing the outer and inner perimeters of the myelin sheaths of all fibers within, and touching north and east borders of, each AOI using Image J software (Abramoff et al., 2004). The perimeter measurements were then converted into diameters (Edgar et al., 2009).

Transverse ultra-thin (80 nm) sections of sciatic nerve were cut using an ultra-microtome equipped with a diamond knife. The sections were collected on coated copper grids and stained with 2% aqueous uranyl acetate for 10 mins and 0.5% lead citrate for 5 mins. Random non-overlapping AOIs (10 per mouse sample) were collected at ~7400x magnification by transmission electron microscopy (Philips CM100). These images were used to trace axonal and mitochondrial cross-sectional areas and to quantify the density of unmyelinated nerve fibers and mitochondrial per myelinated axon cross section in all fibers within, and touching north and east borders of each AOI. Mitochondrial density was calculated by dividing the number of mitochondria per axonal cross-section by the mean axonal cross-sectional area for that genotype. This estimation is based on the assumption that, as in the optic nerve, mitochondria in myelinated axons greater than ~0.7 □m diameter occupy a constant proportion of axonal cytoplasmic volume, independent of axonal diameter (Perge et al., 2009). Analysis of mitochondrial integrity was performed according to (Deighton et al., 2014). Mitochondria were considered normal if cristae were clearly visible and covered >50% of the matrix, abnormal if cristae were absent and/or the mitochondria were swollen, and uncertain if

mitochondria contained slightly fewer cristae than normal but appeared otherwise normal. A minimum of 505 mitochondria were assessed per genotype.

Extracellular sciatic nerve recordings

Mice for electrophysiology were killed by cervical dislocation and the right sciatic nerve trunk was removed from WT and *Mecp2*$^{+/-}$ mice, taking care not to stretch the nerve. Nerves were mounted across 3 chambers in a Perspex recording block and sealed at chamber intervals with vacuum grease for recording. Recordings were performed as described previously (Yao et al., 2014). Briefly, nerve samples were maintained in Ringer's solution and recordings performed at room temperature. Nerves were stimulated at 1 Hz and supramaximal voltage (Grass S88 stimulator; Grass Instruments) for 30 mins to measure conduction velocity (CV). Signals were amplified (CED1902; Cambridge Electronic Design), digitized (NIDAQ-MX analog-to-digital converter; National Instruments), and analyzed using WinWCP version 4.5.2. The distance between the stimulating and recording electrodes was divided by the time between the stimulation artifact and the peak of compound action potential to calculate conduction velocity.

Paired-pulse recordings were performed on the same nerve sample to assess refractoriness. To determine refractoriness, the percentage amplitude of the second waveform, elicited at intervals ranging from 3 to 30 ms, compared with the first was calculated for every inter-stimulus interval. At termination of the experiment, nerve crush was performed to confirm that the recorded waveform originated from real activity.

Statistical and data analysis

Tests for differences between treatment groups were carried out in GraphPad PRISM using a Student's *t*-test, two-way ANOVA or Chi-square test, as

appropriate. $p < 0.05$ was used to define statistical significance. For electrophysiological data, a two-way ANOVA was used to compare CV between genotypes and to compare paired-pulse amplitudes with increasing inter-stimulus interval. For g-ratio plots, non-linear regression analysis and least squares fit was conducted using Graphpad PRISM.

Results

Reduced diameter of myelinated fibers in *Mecp2*$^{+/-}$ mice

In order to establish if the structural and functional properties of peripheral nerve fibers are altered in an RTT model, the sciatic nerve was isolated from 8 month old female *Mecp2*$^{+/-}$ mice (mosaic for functional MeCP2 expression) (n = 9) and wild-type littermates (n = 5). To ensure that the *Mecp2*$^{+/-}$ mouse cohort was symptomatic, mice were scored, prior to collecting tissues, using our standard aggregate phenotype severity scoring system, which is based on the presence of several RTT-like aspects of the phenotype (Guy et al., 2007; Gadalla et al., 2013; Garg et al., 2013). *Post hoc* analysis confirmed that the *Mecp2*$^{+/-}$ mice used showed a significantly higher severity score than the WT group (1.88 ± 0.38 in *Mecp2*$^{+/-}$ vs. 0.20 ± 0.20 in WT mice, mean ± SEM, $p = 0.0098$, unpaired *t* test). In order to exclude the possibility of mouse size as a confounding factor affecting morphological measures, bodyweight and tibial length were measured. However, there was no significant difference in bodyweight (23.88 ± 0.98 g in WT vs. 26.49 ± 1.09 g in *Mecp2*$^{+/-}$, mean ± SEM, $p = 0.14$, unpaired *t* test) or tibial length (17.00 ± 0.24 mm in WT vs. 17.11 ± 0.20 mm in *Mecp2*$^{+/-}$, mean ± SEM, $p = 0.40$, unpaired *t* test) between genotypes.

To assess the diameter of sciatic nerve fibers (axon plus myelin sheath) and their axons, semi-thin sections were prepared from sciatic nerve and stained with Azur

blue (figure 1A). Myelinated fiber diameters in the *Mecp2*$^{+/-}$ mice were significantly reduced compared to WT controls (7.04 ± 0.20 µm and 8.89 ± 0.20 µm respectively, mean ± SEM, $p < 0.001$, unpaired *t* test; figure 1B&C). Similarly, diameters of axons of these myelinated fibers in *Mecp2*$^{+/-}$ mice were significantly reduced compared to WT (4.75 ± 0.20 µm and 6.03 ± 0.10 µm respectively, mean ± SEM, $p < 0.001$, unpaired *t* test; figure 1D&E). As predicted on the basis of reduced diameters, the density of myelinated fibers in the *Mecp2*$^{+/-}$ mice was significantly higher than in the WT ($3.02 \times 10^4 \pm 0.16$ vs. $2.58 \times 10^4 \pm 0.16$ per mm^2, respectively, mean ± SEM, $p = 0.034$, unpaired *t* test, figure 1F). We also estimated myelin thickness through subtraction of axonal diameter from fiber (axon plus myelin) diameter (figure 2A). The myelin thickness was significantly reduced in *Mecp2*$^{+/-}$ mice compared to WT (*Mecp2*$^{+/-}$ = 1.14 ± 0.04 µm, WT = 1.43 ± 0.09 µm, mean ± SEM, $p = 0.006$, unpaired *t* test, figure 2A). However, as all axons within an AOI were measured, these values partially reflect the fact that more small diameter fibers, with comparatively thin myelin sheaths, were quantified in the mutant. Therefore we determined if myelin sheaths were appropriately thick in relation to the diameter of their axons (small axons have thinner sheaths than large axons) by plotting g-ratio (ratio of axon diameter to fiber diameter) against axonal diameter (figure 2B). This revealed *Mecp2*$^{+/-}$ axons to have slightly thinner than normal myelin sheaths (higher g-ratio) across the entire range of axon diameters. Pearson r values for axonal diameter versus g-ratio for WT fibers was 0.619 and for *Mecp2*$^{+/-}$ fibers was 0.605, indicating a strong correlation between axonal diameter and g-ratio for both genotypes ($p < 0.0001$ for both WT and *Mecp2*$^{+/-}$).

Density and diameter of unmyelinated axons in *Mecp2*$^{+/-}$ mice are not altered

To examine unmyelinated axons in the sciatic nerve, transverse ultrathin sections of nerve from *Mecp2*$^{+/-}$ and WT mice were imaged by transmission electron microscopy (figure 3A-C). There was no significant difference in the diameter of the unmyelinated axons between WT and *Mecp2*$^{+/-}$ mice (0.73 ± 0.01 µm vs. 0.71 ± 0.02 µm, respectively, mean ± SEM, $p = 0.62$, unpaired *t* test). There was also no difference in the density of unmyelinated axons between genotypes (1.86 ± 0.28 x 10^5 axons/mm^2 and 2.32 ± 0.44 x 10^5 axons/mm^2 for WT and *Mecp2*$^{+/-}$, respectively, mean ± SEM, $p = 0.4$, unpaired *t* test).

Mitochondrial densities per unit area of axoplasm are increased in *Mecp2*$^{+/-}$ mice.

Mitochondrial dysfunction has been previously reported in muscle biopsies from RTT patients (Wakai et al., 1990) and in the central nervous system of *Mecp2*-null mice (Grosser et al., 2012; De Filippis et al., 2015). We therefore investigated whether mitochondrial density was altered in sciatic nerve myelinated axons in *Mecp2*$^{+/-}$ mice (figure 4A). Electron microscopic analysis revealed that the number of mitochondria per myelinated axon cross section in the sciatic nerve sections of *Mecp2*$^{+/-}$ mice was significantly reduced compared to WT samples (1.62 ± 0.10 and 2.02 ± 0.12 mitochondria per axon cross section, respectively, mean ± SEM, $p = 0.03$, unpaired *t* test, figure 4B). In contrast, the density of mitochondria per mm^2 of axoplasm of myelinated axons was significantly higher in the *Mecp2*$^{+/-}$ compared to WT mice (95.43 ± 6.81 x 10^3 and 70.96 ± 3.94 x 10^3 mitochondria per mm^2, respectively, mean ± SEM, $p = 0.012$, unpaired *t* test; figure 4C). Unlike the differences observed above, there was no difference in mitochondrial morphology between *Mecp2*$^{+/-}$ and WT mice (normal morphology; 87.06 ± 2.31% and 89 ± 0.95%, abnormal; 7.73 ± 1.50% and 8.71 ±1.07%, uncertain; 5.21 ± 1.41% and 2.28 ±1.01%, respectively, mean ± SEM, $p > 0.05$, Chi-square test, figure 5A&B).

Further, there was no difference in the mean diameter of axonal mitochondria between the genotypes (WT = 0.31± 0.02 µm vs. *Mecp2*$^{+/-}$ = 0.34 ± 0.02 µm, mean ± SEM, $p = 0.19$, unpaired *t* test; figure 5C).

Conduction properties of the sciatic nerve of *Mecp2*$^{+/-}$ mice are unaltered

To test sciatic nerve conduction properties, 10 mm segments were collected immediately after death and mounted for electrophysiological extracellular recording. There was no difference in conduction velocity between genotypes across a range of stimulus intensities ($p > 0.05$, two-way ANOVA, figure 6 A&B). Similarly, paired-pulse stimulation revealed no difference in the refractory period between genotypes when tested across a range of inter-stimulus intervals ($p > 0.05$, two-way ANOVA, figure 6C).

Discussion

In this study, we utilized morphometric and electrophysiological techniques to assess potential abnormalities in peripheral nerve structure and function arising from MeCP2 deficiency. We focused our study on symptomatic *Mecp2*-heterozygous female mice as these model the genetic and molecular changes in RTT patients most accurately. Our main findings are the observed differences in the sciatic nerve fiber diameter and density, as well as the altered mitochondrial density in the myelinated axons of *Mecp2*$^{+/-}$ mice. However, other morphological features such as density and diameter of unmyelinated axons were unaltered and we did not detect any functional impairment in terms of nerve conduction in whole nerve recordings. The sciatic nerve contains motor, sensory and autonomic nerve fibers and it is possible that the average values we obtained reflect a preferential effect on one or more of these populations. However, it is not possible in micrographs of resin sections or in electron micrographs to distinguish, with

certainty, the fiber subtypes. Therefore, it is possible that certain populations were more affected by MeCP2 deficiency than others. We cannot exclude the possibility that the absence of detectable differences in conduction velocity in *ex vivo* nerve segments is related to the subtlety of the ultrastructural changes in the fiber diameters and the relatively short length of the mouse nerve preparation used for the electrophysiological studies (10 mm). However, nerve conduction velocity studies in patients, even in advanced stages of RTT, suggest only slight signs of peripheral nerve damage/dysfunction (Glaze, 2005).

This, the first report of peripheral nerve phenotypes in mice modelling RTT, is broadly consistent with early clinical data showing ultrastructural abnormalities in the sural nerve, including a reduction in numbers of large myelinated fibers and mitochondrial alterations in myelinated axons (Wakai et al., 1990). We did not observe evidence of axonal degeneration, as previously reported in a number of human subjects (Haas and Love, 1988). However, this might reflect the fact that lifespan and peripheral nerve lengths are considerably shorter in mice than in humans, as both increasing age and axonal length are factors influencing the likelihood of occurrence of axonal pathology (Coleman, 2005; Adalbert and Coleman, 2013).

In the current study, we observed myelinated fibers of reduced diameter in *Mecp2*$^{+/-}$ mouse sciatic nerves (Figs 1 b, d and f). This was due to reductions in both axonal diameter and myelin sheath thickness (as shown by increased g-ratio), In other respects, Schwann cells appeared normal in *Mecp2*$^{+/-}$ mice including well compacted myelin, lack of redundant myelin or tomaculae, and healthy-appearing Schwann cell nuclei (data not shown). Nonetheless, we do not exclude the possibility of other changes that were not assessed in this study. For example, Pi-granules (metachromatic granules) and swollen mitochondria have been reported in

the cytoplasm of Schwann cells in clinical biopsies from RTT patients (Wakai et al., 1990).

Multiple factors play a role in Schwann cell differentiation and myelination (Sherman and Brophy, 2005), but one factor in particular, neuregulin-1 (NRG1) type III, fine-tunes myelin sheath thickness to axon caliber (Michailov et al., 2004; Taveggia et al., 2005). Therefore, it will be interesting to determine if the slightly decreased myelin thickness (increased g-ratios) in *Mecp2*$^{+/-}$ sciatic nerves is mirrored by a reduction in *Nrg1* expression in *Mecp2*$^{+/-}$ mouse neurons or whether this myelin phenotype reflects a Schwann cell autonomous effect. It is possible that the reduced axonal diameter in the RTT mouse model reflects a reduced arborisation of axon terminals per fiber (Perge et al., 2009), but analysis of terminals was beyond the scope of our study.

Axonal mitochondria provide the energy required for motor protein-driven axonal transport and for ion exchange through Na/K-ATPases that are located on the intermodal axolemma (Mata et al., 1991; McGrail et al., 1991; Alberti et al., 2007; Young et al., 2008). In myelinated sciatic nerve fibers of both WT and *Mecp2*$^{+/-}$ mice, the mean axonal mitochondrial diameter was ~0.32 □m. In comparison, the mean diameter of optic nerve axonal mitochondria is ~0.22 □m (Perge et al., 2009). While tissue processing for electron microscopy will cause some degree of shrinkage that will vary according to the methodology, these size differences probably reflect mainly the fact that large caliber axons (as in the sciatic nerve) have a greater energy requirement per unit volume than small caliber axons, as in the optic nerve.

At least in optic nerve axons, total mitochondrial volume (Vm) scales roughly in proportion to axonal diameter squared (Perge et al., 2009), and for axons > 0.7 □m

in diameter, mitochondria therefore make up a constant proportion (~ 1.5%) of axoplasm volume, independent of axonal diameter. In other words, the number of mitochondria per axon should scale with axonal volume (and hence with axonal cross-sectional area, if we treat axons as regular cylinders). Although the density of mitochondria per unit cross-sectional area is higher in *Mecp2*$^{+/-}$ mice than in WT mice, the increase is not in proportion given the ratio of diameters in the two genotypes (the axon diameter ratio is 1:1.27; the mitochondrial density should therefore scale with diameter squared i.e. 1.61:1; the observed ratio of mitochondrial densities is only 1.34:1). On the assumption that the mitochondria are the same length and have the same orientation relative the axonal long axis in the two genotypes, we therefore conclude that there may be fewer mitochondria per myelinated axon in *Mecp2*$^{+/-}$ mice. This interesting observation needs to be followed up in more detailed studies of mitochondrial function in peripheral nerves in RTT models.

Previous research on mice modeling RTT has focused on studying dysfunction within the central nervous system and revealed a variety of cellular and network features associated with MeCP2-deficiency, such as imbalance between cortical excitatory and inhibitory circuits (Dani et al., 2005), diminished synaptic plasticity (Asaka et al., 2006; Weng et al., 2011), as well as aberrant EEG (D'Cruz et al., 2010), seizures (McLeod et al., 2013) and brainstem dysfunction leading to abnormal breathing patterns (Viemari et al., 2005). However, certain cardinal features of RTT in mouse models, such as hindlimb clasping (Shahbazian et al., 2002; Guy et al., 2007; Gadalla et al., 2013) and gait abnormalities (Guy et al., 2007; Gadalla et al., 2014), could potentially be a consequence of combined abnormalities of both central and peripheral nervous systems. Mouse models in which *Mecp2* is selectively silenced either in the nervous system (Guy et al., 2001)

or in peripheral tissue (Luikenhuis et al., 2004; Ross et al., 2016), highlighted the pivotal role of the nervous system in the development of prominent RTT like phenotypes. However, these experiments do not discriminate the relative contribution of MeCP2 deficiency in peripheral nerves and the potential role of peripheral nerve dysfunction has generally been neglected, despite the early reported cases of peripheral nerve abnormalities in RTT patients, prior to the discovery of the genetic basis of the disorder (Haas and Love, 1988; Wakai et al., 1990). The changes in sciatic nerve morphology of *Mecp2*$^{+/-}$ mice in this study are similar to those reported in several animal models of other neurological conditions that are primarily considered to be brain disorders (Wade et al., 2008; Lopes et al., 2016). Moreover, reduced axonal diameter in peripheral nerves has also been reported in IGF1-deficient mice, a phenotype that was reversed following IGF1 administration (Gao et al., 1999). This could be relevant in RTT where IGF1 tripeptide administration has been shown to rescue locomotion as well as structural abnormalities within the brain of *Mecp2*-null mice (Tropea et al., 2009).

In conclusion, we report modest structural abnormalities in the peripheral nerves of *Mecp2*$^{+/-}$ mice. The reduced axonal diameter mirrors morphological alterations seen in the brain, and could potentially contribute to certain RTT-like phenotypes.

Author contributions

Conceived and designed the experiments: SC, KG, JE, NB. Performed the experiments: NB, KG, RM. Analyzed the data: NB, KG, RM. Wrote the paper: SC, MB, KG, JE, NB, RM.

Acknowledgments

This work was supported by Rett Syndrome Research Trust, Rett Syndrome Association Scotland, the R.S. MacDonald Charitable Trust, the Stoneygate Trust and the Rosetrees Trust. We are grateful to Janos Perge for helpful discussion on the interpretation of morphological data.

References

Adalbert R, Coleman MP (2013) Review: Axon pathology in age-related neurodegenerative disorders. Neuropathol Appl Neurobiol 39:90-108.

Alberti S, Gregorio EA, Spadella CT, Cojocel C (2007) Localization and irregular distribution of Na,K-ATPase in myelin sheath from rat sciatic nerve. Tissue Cell 39:195-201.

Armstrong D, Dunn JK, Antalffy B, Trivedi R (1995) Selective dendritic alterations in the cortex of Rett syndrome. J Neuropathol Exp Neurol 54:195-201.

Asaka Y, Jugloff DG, Zhang L, Eubanks JH, Fitzsimonds RM (2006) Hippocampal synaptic plasticity is impaired in the Mecp2-null mouse model of Rett syndrome. Neurobiol Dis 21:217-227.

Bauman ML, Kemper TL, Arin DM (1995) Pervasive neuroanatomic abnormalities of the brain in three cases of Rett's syndrome. Neurology 45:1581-1586.

Chen RZ, Akbarian S, Tudor M, Jaenisch R (2001) Deficiency of methyl-CpG binding protein-2 in CNS neurons results in a Rett-like phenotype in mice. Nat Genet 27:327-331.

Coleman M (2005) Axon degeneration mechanisms: commonality amid diversity. Nat Rev Neurosci 6:889-898.

D'Cruz JA, Wu C, Zahid T, El-Hayek Y, Zhang L, Eubanks JH (2010) Alterations of cortical and hippocampal EEG activity in MeCP2-deficient mice. Neurobiol Dis 38:8-16.

Dani VS, Chang Q, Maffei A, Turrigiano GG, Jaenisch R, Nelson SB (2005) Reduced cortical activity due to a shift in the balance between excitation and inhibition in a mouse model of Rett syndrome. Proc Natl Acad Sci U S A 102:12560-12565.

De Filippis B, Valenti D, de Bari L, De Rasmo D, Musto M, Fabbri A, Ricceri L, Fiorentini C, Laviola G, Vacca RA (2015) Mitochondrial free radical

overproduction due to respiratory chain impairment in the brain of a mouse model of Rett syndrome: protective effect of CNF1. Free Radic Biol Med 83:167-177.
Deighton RF, Le Bihan T, Martin SF, Gerth AM, McCulloch M, Edgar JM, Kerr LE, Whittle IR, McCulloch J (2014) Interactions among mitochondrial proteins altered in glioblastoma. J Neurooncol 118:247-256.
Edgar JM, McLaughlin M, Werner HB, McCulloch MC, Barrie JA, Brown A, Faichney AB, Snaidero N, Nave KA, Griffiths IR (2009) Early ultrastructural defects of axons and axon-glia junctions in mice lacking expression of Cnp1. Glia 57:1815-1824.
Gadalla KK, Bailey ME, Cobb SR (2011) MeCP2 and Rett syndrome: reversibility and potential avenues for therapy. Biochem J 439:1-14.
Gadalla KK, Ross PD, Riddell JS, Bailey ME, Cobb SR (2014) Gait analysis in a Mecp2 knockout mouse model of Rett syndrome reveals early-onset and progressive motor deficits. PLoS One 9:e112889.
Gadalla KK, Bailey ME, Spike RC, Ross PD, Woodard KT, Kalburgi SN, Bachaboina L, Deng JV, West AE, Samulski RJ, Gray SJ, Cobb SR (2013) Improved survival and reduced phenotypic severity following AAV9/MECP2 gene transfer to neonatal and juvenile male Mecp2 knockout mice. Mol Ther 21:18-30.
Gao WQ, Shinsky N, Ingle G, Beck K, Elias KA, Powell-Braxton L (1999) IGF-I deficient mice show reduced peripheral nerve conduction velocities and decreased axonal diameters and respond to exogenous IGF-I treatment. J Neurobiol 39:142-152.
Garg SK, Lioy DT, Cheval H, McGann JC, Bissonnette JM, Murtha MJ, Foust KD, Kaspar BK, Bird A, Mandel G (2013) Systemic delivery of MeCP2 rescues behavioral and cellular deficits in female mouse models of Rett syndrome. J Neurosci 33:13612-13620.
Gillespie MJ, Stein RB (1983) The relationship between axon diameter, myelin thickness and conduction velocity during atrophy of mammalian peripheral nerves. Brain Res 259:41-56.
Glaze DG (2005) Neurophysiology of Rett syndrome. J Child Neurol 20:740-746.
Grosser E, Hirt U, Janc OA, Menzfeld C, Fischer M, Kempkes B, Vogelgesang S, Manzke TU, Opitz L, Salinas-Riester G, Muller M (2012) Oxidative burden and mitochondrial dysfunction in a mouse model of Rett syndrome. Neurobiol Dis 48:102-114.
Guy J, Hendrich B, Holmes M, Martin JE, Bird A (2001) A mouse Mecp2-null mutation causes neurological symptoms that mimic Rett syndrome. Nat Genet 27:322-326.

Guy J, Gan J, Selfridge J, Cobb S, Bird A (2007) Reversal of neurological defects in a mouse model of Rett syndrome. Science 315:1143-1147.
Haas RH, Love S (1988) Peripheral nerve findings in Rett syndrome. J Child Neurol 3 Suppl:S25-30.
Leonard H, Cobb S, Downs J (2017) Clinical and biological progress over 50 years in Rett syndrome. Nat Rev Neurol 13:37-51.
Lopes S, Lopes A, Pinto V, Guimaraes MR, Sardinha VM, Duarte-Silva S, Pinheiro S, Pizarro J, Oliveira JF, Sousa N, Leite-Almeida H, Sotiropoulos I (2016) Absence of Tau triggers age-dependent sciatic nerve morphofunctional deficits and motor impairment. Aging Cell 15:208-216.

Lyst MJ, Bird A (2015) Rett syndrome: a complex disorder with simple roots. Nat Rev Genet 16:261-275.
Mata M, Fink DJ, Ernst SA, Siegel GJ (1991) Immunocytochemical demonstration of Na+,K(+)-ATPase in internodal axolemma of myelinated fibers of rat sciatic and optic nerves. J Neurochem 57:184-192.
McGrail KM, Phillips JM, Sweadner KJ (1991) Immunofluorescent localization of three Na,K-ATPase isozymes in the rat central nervous system: both neurons and glia can express more than one Na,K-ATPase. J Neurosci 11:381-391.
McLeod F, Ganley R, Williams L, Selfridge J, Bird A, Cobb SR (2013) Reduced seizure threshold and altered network oscillatory properties in a mouse model of Rett syndrome. Neuroscience 231:195-205.
Michailov GV, Sereda MW, Brinkmann BG, Fischer TM, Haug B, Birchmeier C, Role L, Lai C, Schwab MH, Nave KA (2004) Axonal neuregulin-1 regulates myelin sheath thickness. Science 304:700-703.
Neul JL, Kaufmann WE, Glaze DG, Christodoulou J, Clarke AJ, Bahi-Buisson N, Leonard H, Bailey ME, Schanen NC, Zappella M, Renieri A, Huppke P, Percy AK, RettSearch C (2010) Rett syndrome: revised diagnostic criteria and nomenclature. Ann Neurol 68:944-950.
Nguyen MV, Du F, Felice CA, Shan X, Nigam A, Mandel G, Robinson JK, Ballas N (2012) MeCP2 is critical for maintaining mature neuronal networks and global brain anatomy during late stages of postnatal brain development and in the mature adult brain. J Neurosci 32:10021-10034.
Perge JA, Koch K, Miller R, Sterling P, Balasubramanian V (2009) How the optic nerve allocates space, energy capacity, and information. J Neurosci 29:7917-7928.
Robinson L, Guy J, McKay L, Brockett E, Spike RC, Selfridge J, De Sousa D, Merusi C, Riedel G, Bird A, Cobb SR (2012) Morphological and functional

reversal of phenotypes in a mouse model of Rett syndrome. Brain 135:2699-2710.
Ross PD, Guy J, Selfridge J, Kamal B, Bahey N, Tanner KE, Gillingwater TH, Jones RA, Loughrey CM, McCarroll CS, Bailey ME, Bird A, Cobb S (2016) Exclusive expression of MeCP2 in the nervous system distinguishes between brain and peripheral Rett syndrome-like phenotypes. Hum Mol Genet.
Ruch A, Kurczynski TW, Velasco ME (1989) Mitochondrial alterations in Rett syndrome. Pediatr Neurol 5:320-323.
Shahbazian M, Young J, Yuva-Paylor L, Spencer C, Antalffy B, Noebels J, Armstrong D, Paylor R, Zoghbi H (2002) Mice with truncated MeCP2 recapitulate many Rett syndrome features and display hyperacetylation of histone H3. Neuron 35:243-254.
Taveggia C, Zanazzi G, Petrylak A, Yano H, Rosenbluth J, Einheber S, Xu X, Esper RM, Loeb JA, Shrager P, Chao MV, Falls DL, Role L, Salzer JL (2005) Neuregulin-1 type III determines the ensheathment fate of axons. Neuron 47:681-694.
Tropea D, Giacometti E, Wilson NR, Beard C, McCurry C, Fu DD, Flannery R, Jaenisch R, Sur M (2009) Partial reversal of Rett Syndrome-like symptoms in MeCP2 mutant mice. Proc Natl Acad Sci U S A 106:2029-2034.
Viemari JC, Maussion G, Bevengut M, Burnet H, Pequignot JM, Nepote V, Pachnis V, Simonneau M, Hilaire G (2005) Ret deficiency in mice impairs the development of A5 and A6 neurons and the functional maturation of the respiratory rhythm. Eur J Neurosci 22:2403-2412.
Wade A, Jacobs P, Morton AJ (2008) Atrophy and degeneration in sciatic nerve of presymptomatic mice carrying the Huntington's disease mutation. Brain Res 1188:61-68.
Wakai S, Kameda K, Ishikawa Y, Miyamoto S, Nagaoka M, Okabe M, Minami R, Tachi N (1990) Rett syndrome: findings suggesting axonopathy and mitochondrial abnormalities. Pediatr Neurol 6:339-343.
Weng SM, McLeod F, Bailey ME, Cobb SR (2011) Synaptic plasticity deficits in an experimental model of rett syndrome: long-term potentiation saturation and its pharmacological reversal. Neuroscience 180:314-321.
Yao D, McGonigal R, Barrie JA, Cappell J, Cunningham ME, Meehan GR, Fewou SN, Edgar JM, Rowan E, Ohmi Y, Furukawa K, Furukawa K, Brophy PJ, Willison HJ (2014) Neuronal expression of GalNAc transferase is sufficient to prevent the age-related neurodegenerative phenotype of complex ganglioside-deficient mice. J Neurosci 34:880-891.
Young EA, Fowler CD, Kidd GJ, Chang A, Rudick R, Fisher E, Trapp BD (2008) Imaging correlates of decreased axonal Na+/K+ ATPase in chronic multiple sclerosis lesions. Ann Neurol 63:428-435.

Figure legends

Figure 1. The diameter of nerve fibers and their axons is reduced in *Mecp2*$^{+/-}$ mice

(A) Representative micrographs of Azur blue stained semi-thin transverse sections of the sciatic nerve, illustrating myelinated nerve fibers in WT (left) and *Mecp2*$^{+/-}$ mice (right). Graphs showing (B) mean fiber diameter, (C) fiber diameter frequency distribution, (D) mean axon diameter, (E) axon diameter frequency distribution, (F) plot showing mean density of myelinated axons within the sciatic nerve. Data are presented as mean ± S.E.M. (n=5 WT and 9 *Mecp2*$^{+/-}$ mice). Unpaired Student's *t* test was used to compare genotypes.* $p < 0.05$, *** $p \leq 0.0001$.

Figure 2. Analysis of g-ratio in sciatic nerve of *Mecp2*$^{+/-}$ mice

(A) Plot showing mean myelin thickness. (B) Plot of g-ratio versus axonal diameter. Note there is a tendency for a higher g-ratio (thinner than normal myelin) across all axon diameters in *Mecp2*$^{+/-}$ compared to control samples. In B, each point represents a single fiber. Data in A are presented as mean ± S.E.M. (n=5 WT and 9 *Mecp2*$^{+/-}$ mice). Unpaired Student's *t* test was used to compare genotypes.** $p < 0.01$.

Figure 3. The density of unmyelinated axons in *Mecp2*$^{+/-}$ mouse sciatic nerve is unaltered

(A) Transmission electron micrographs of transverse section of the sciatic nerve showing myelinated (m) and unmyelinated axons (white arrows). Graph showing (B) mean diameter of unmyelinated axons and (C) density of unmyelinated fibers. Data are presented as mean ± SEM (n = 5 WT and 7 *Mecp2*$^{+/-}$ mice). Unpaired *t* test was used to compare genotypes. Abbreviations: m: myelin; sc: Schwann cell nucleus; ax: axon.

Figure 4. The number of mitochondria per myelinated axon cross-section is reduced in *Mecp2*$^{+/-}$ mice

(A) Transmission electron micrographs of transverse sections of the sciatic nerve showing mitochondria (arrows) in the axoplasm of myelinated (m) axons (ax). Graphs showing (B) the mean number of mitochondria per myelinated axon, (C) mean number of mitochondria per mm^2 of the axoplasm of myelinated axons. Data are presented as mean ± SEM (n = 5 WT and 7 *Mecp2*$^{+/-}$ mice). Unpaired *t* test was used to compare genotypes. * $p < 0.05$.

Figure 5. Axonal mitochondria appear normal in *Mecp2*$^{+/-}$ mice

(A) Electron micrograph showing normal (black arrow) and abnormal (swollen and lacking cristae; white arrows). (B) Plot showing percentage of mitochondria in myelinated axons designated normal, abnormal or uncertain. (C) Plot showing mean cross-sectional diameter of axonal mitochondria. Data are presented as mean ± SEM (n = 5 WT and 7 *Mecp2*$^{+/-}$ mice). There was no difference between genotypes in B (Chi-square test on raw counts) or C (unpaired unpaired *t*-test), all $p > 0.05$, ns = not significant.

Figure 6. Normal sciatic nerve conduction properties in *Mecp2*$^{+/-}$ mice

(A) Representative evoked compound action potentials in sciatic nerve from 10 months old WT (n = 5) and *Mecp2*$^{+/-}$ (n = 6) mice. (B) Plot showing no difference in conduction velocity between genotypes over increasing stimulus intensity ($p > 0.05$, two-way ANOVA). (C) Plot of paired-pulse data showing the relative amplitude of the second pulse over varying inter-stimulus intervals. There was no change to refractory period between genotypes ($p > 0.05$, two-way ANOVA).

Research Highlights

- A mouse model of Rett syndrome reveals a reduced diameter of peripheral myelinated nerve fibers
- Mitochondrial densities per unit area of axoplasm are significantly altered in *Mecp2*$^{+/-}$ mice
- There is no detectable change in mitochondrial integrity or nerve conduction properties between *Mecp2*$^{+/-}$ and wild-type mice

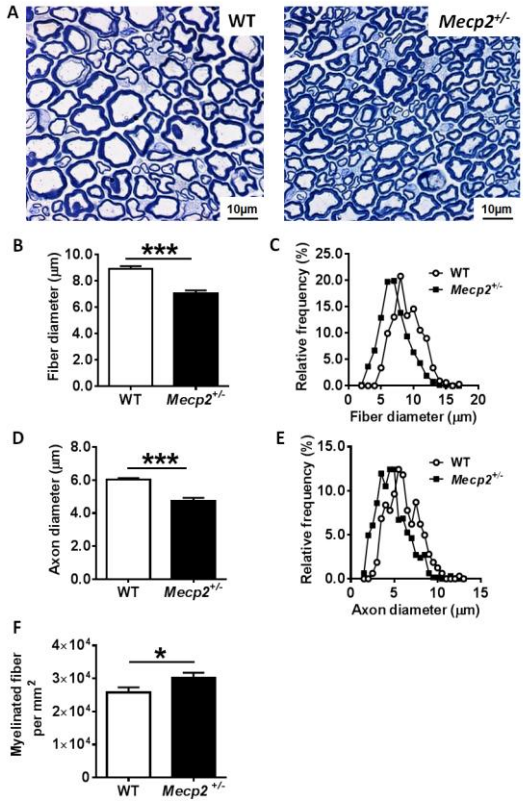
A
WT
Mecp2+/-
10μm
10μm
B
Fiber diameter (μm)
***
WT
Mecp2+/-
C
Relative frequency (%)
WT
Mecp2+/-
Fiber diameter (μm)
D
Axon diameter (μm)
***
WT
Mecp2+/-
E
Relative frequency (%)
WT
Mecp2+/-
Axon diameter (μm)
F
Myelinated fiber per mm2
*
WT
Mecp2+/-

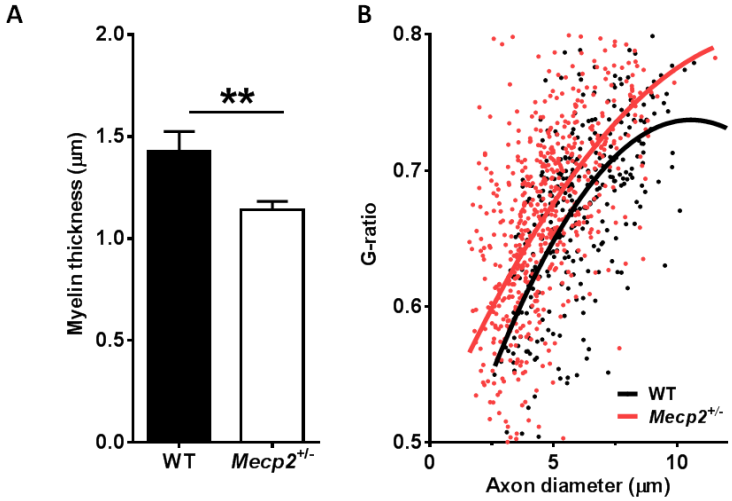
A
2.0
1.5
1.0
0.5
0.0
Myelin thickness (μm)
**
WT
Mecp2+/-
B
0.8
0.7
0.6
0.5
G-ratio
0
5
10
Axon diameter (μm)
WT
Mecp2+/-

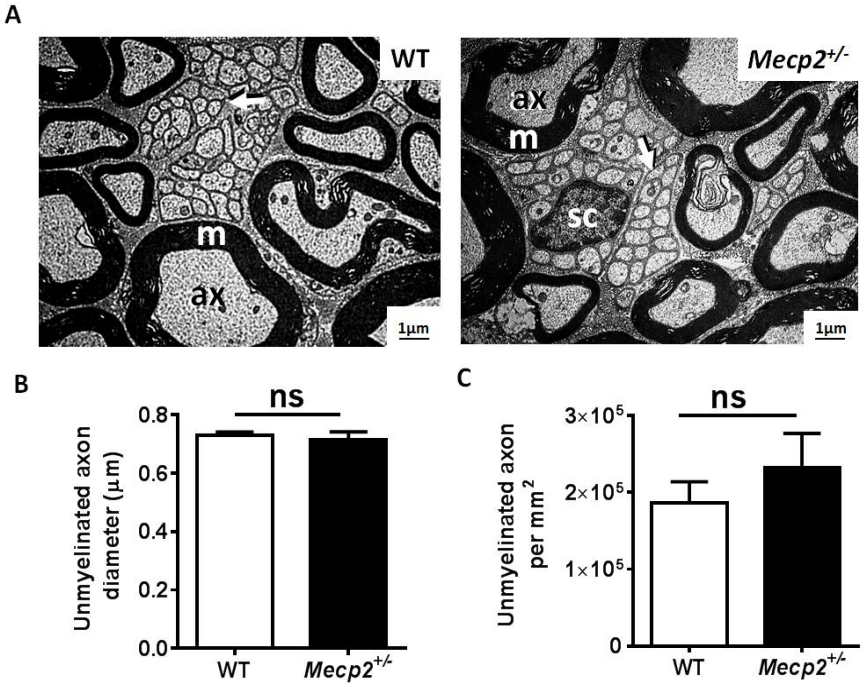
A
WT
Mecp2+/-
ax
m
sc
1µm
1µm
B
ns
Unmyelinated axon diameter (µm)
0.8
0.6
0.4
0.2
0.0
WT
Mecp2+/-
C
ns
Unmyelinated axon per mm2
3×10^5
2×10^5
1×10^5
0
WT
Mecp2+/-

A

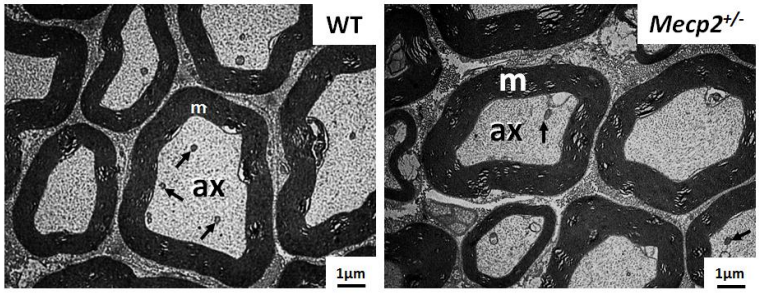
WT
m
ax
1µm
Mecp2+/-
m
ax
1µm

B

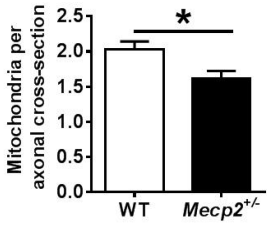
Mitochondria per axonal cross-section
2.5
2.0
1.5
1.0
0.5
0.0
*
WT
Mecp2+/-

C

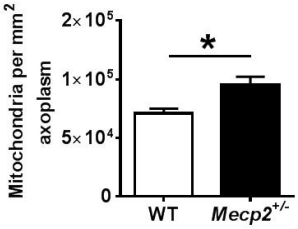
Mitochondria per mm2 axoplasm
2×10^5
1×10^5
5×10^4
0
*
WT
Mecp2+/-

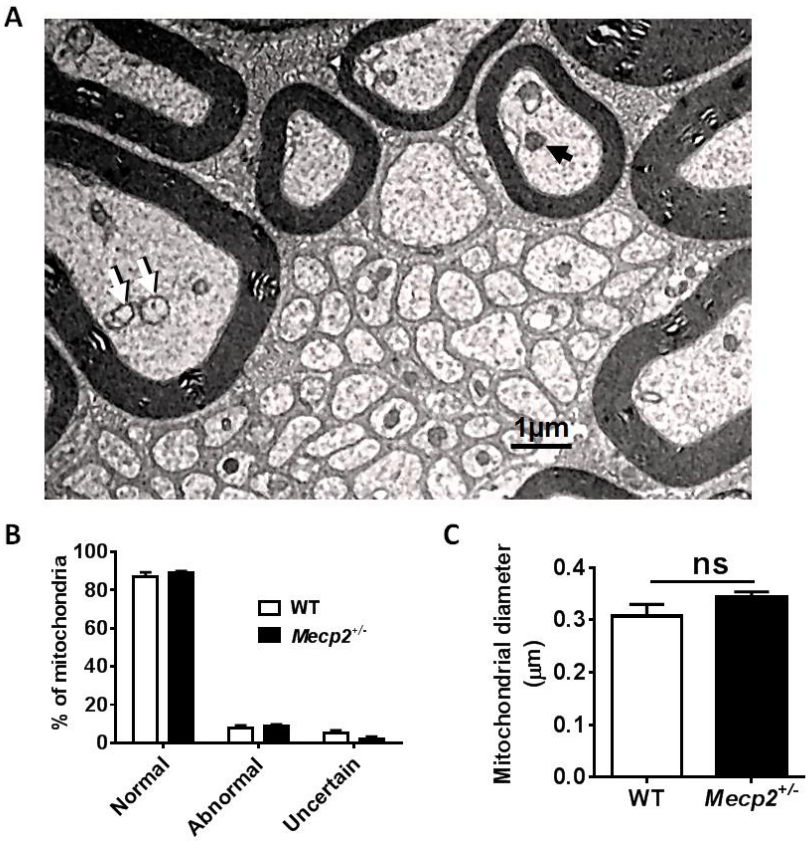
A
1μm
B
% of mitochondria
100
80
60
40
20
0
WT
Mecp2+/-
Normal
Abnormal
Uncertain
C
Mitochondrial diameter (μm)
0.4
0.3
0.2
0.1
0.0
ns
WT
Mecp2+/-

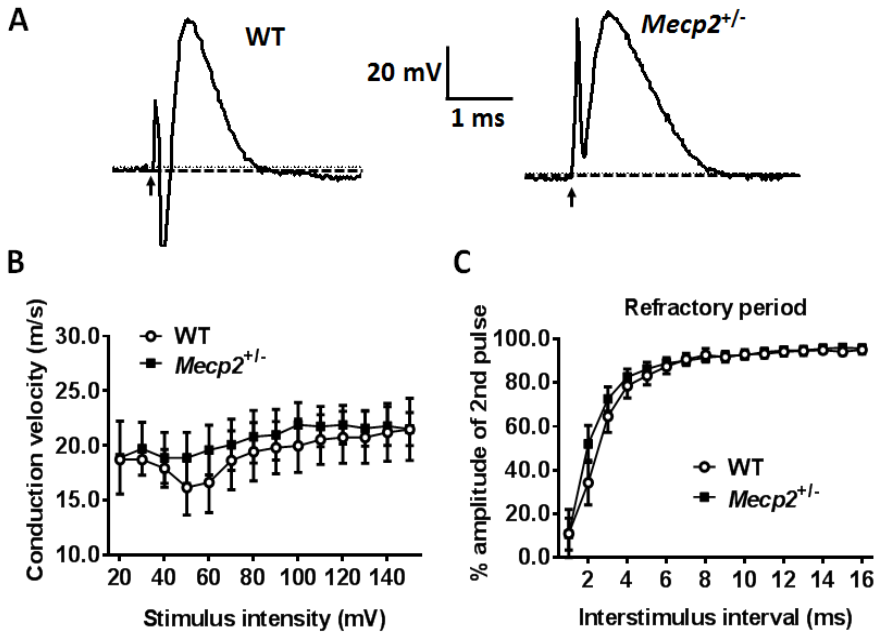
A
WT
Mecp2+/-
20 mV
1 ms
B
Conduction velocity (m/s)
30.0
25.0
20.0
15.0
10.0
WT
Mecp2+/-
20 40 60 80 100 120 140
Stimulus intensity (mV)
C
Refractory period
% amplitude of 2nd pulse
100.0
80.0
60.0
40.0
20.0
0.0
WT
Mecp2+/-
2 4 6 8 10 12 14 16
Interstimulus interval (ms)

Graphical abstract